Since January 2020 Elsevier has created a COVID-19 resource centre with free information in English and Mandarin on the novel coronavirus COVID-19. The COVID-19 resource centre is hosted on Elsevier Connect, the company's public news and information website.

Cell Host & Microbe
Article

Entry of Bunyaviruses into Mammalian Cells

Pierre-Yves Lozach,[1] Roberta Mancini,[1] David Bitto,[1] Roger Meier,[1] Lisa Oestereich,[1] Anna K. Överby,[2,3] Ralf F. Pettersson,[2] and Ari Helenius[1,*]
[1]ETH Zurich, Institute of Biochemistry, Schafmattstrasse 18, CH-8093 Zurich, Switzerland
[2]Ludwig Institute for Cancer Research, Stockholm Branch, Karolinska Institute, Box 10 240, SE-17177 Stockholm, Sweden
[3]Department of Virology, University of Freiburg, D-79008 Freiburg, Germany
*Correspondence: ari.helenius@bc.biol.ethz.ch
DOI 10.1016/j.chom.2010.05.007

SUMMARY

The *Bunyaviridae* constitute a large family of enveloped animal viruses, many members of which cause serious diseases. However, early bunyavirus-host cell interactions and entry mechanisms remain largely uncharacterized. Investigating Uukuniemi virus, a bunyavirus of the genus *Phlebovirus*, we found that virus attachment to the cell surface was specific but inefficient, with 25% of bound viruses being endocytosed within 10 min, mainly via non-coated vesicles. The viruses entered Rab5a+ early endosomes and, subsequently, Rab7a+ and LAMP-1+ late endosomes. Acid-activated penetration, occurring 20–40 min after internalization, required maturation of early to late endosomes. The pH threshold for viral membrane fusion was 5.4, and entry was sensitive to temperatures below 25°C. Together, our results indicate that Uukuniemi virus penetrates host cells by acid-activated membrane fusion from late endosomal compartments. This study also highlights the importance of the degradative branch of the endocytic pathway in facilitating entry of late-penetrating viruses.

INTRODUCTION

The *Bunyaviridae* family comprises five genera (*Orthobunyavirus*, *Phlebovirus*, *Nairovirus*, *Hantavirus*, and *Tospovirus*) with more than 350 members worldwide (Schmaljohn and Nichol, 2007). With the exception of hantaviruses, bunyaviruses are transmitted by arthropod vectors and consequently belong to the superfamily of *ar*thropod-*bo*rne viruses (arboviruses). Many are human pathogens and cause severe pathologies such as fatal hepatitis, hemorrhagic fever, encephalitis, and acute fever. Due to their mode of transmission, they are considered potential agents of emerging diseases. No treatments or vaccines are currently approved by the FDA for human use.

Bunyaviruses are enveloped and have a trisegmented, negative-sense RNA genome that replicates in the cytosol (Schmaljohn and Nichol, 2007). Electron microscopy (EM) pictures of viruses show roughly spherical particles with a diameter between 80 and 140 nm and spike-like projections of 5–10 nm (Overby et al., 2008; Schmaljohn and Nichol, 2007). The spikes are composed of the two transmembrane glycopolypeptides, G_N and G_C, responsible for the attachment of the virus to the target cells (Overby et al., 2008). In addition, the C-terminal tails of glycoproteins G_N and G_C are likely to interact inside the viral particles with the ribonucleoproteins (RNPs) composed of the viral RNAs and the N protein (Overby et al., 2008).

The receptors, cellular factors, and pathways used by bunyaviruses to enter their host cells remain largely unidentified and poorly characterized. Inhibitor studies have suggested that orthobunya-, nairo-, and hantaviruses depend on endocytosis internalization and vacuolar acidification. Perturbation of clathrin and dynamin-2 function has implied a role for clathrin-mediated endocytosis (CME) (Jin et al., 2002; Santos et al., 2008; Simon et al., 2009b). In addition, it has been recently proposed that Crimean Congo hemorrhagic fever virus (CCHFV), a nairovirus, requires functional microtubules for infection (Simon et al., 2009a).

We focus here on Uukuniemi virus (UUKV). UUKV belongs to the genus *Phlebovirus* and is thus related to Rift Valley fever virus (RVFV), an important human pathogen (Pettersson and Kaariainen, 1973). Little information is available on *Phlebovirus* entry. Low pH has been shown to affect the biochemical properties of the UUKV glycoproteins and induces fusion of cells expressing the glycoproteins of RVFV (Filone et al., 2006; Overby et al., 2008). This suggests that host cell entry of phleboviruses is dependent on low pH. To analyze the entry of UUKV into mammalian tissue culture cells, we developed sensitive, quantitative tools and assays that allowed us to determine general properties of the UUKV entry process including binding, internalization, membrane trafficking, and acid-activated penetration.

RESULTS

Quantification of Infected Cells by Flow Cytometry

We developed a fluorescence-activated cell sorter (FACS)-based assay to quantify UUKV infection as described in Figure S1, available online. Using this assay, we found that a complete cycle, from infection to release of infectious progeny, lasted about 7 hr in BHK-21 cells. In all the further experiments, we used the antibody 8B11A3 against the N protein to monitor infection and limited our assay to a single infectious cycle by harvesting cells 7 hr after exposure to the virus.

Only BHK-21 and embryonic chicken cells have been reported to support productive UUKV infection (Pettersson and Kaariainen, 1973). We assessed 15 cell lines from different species and

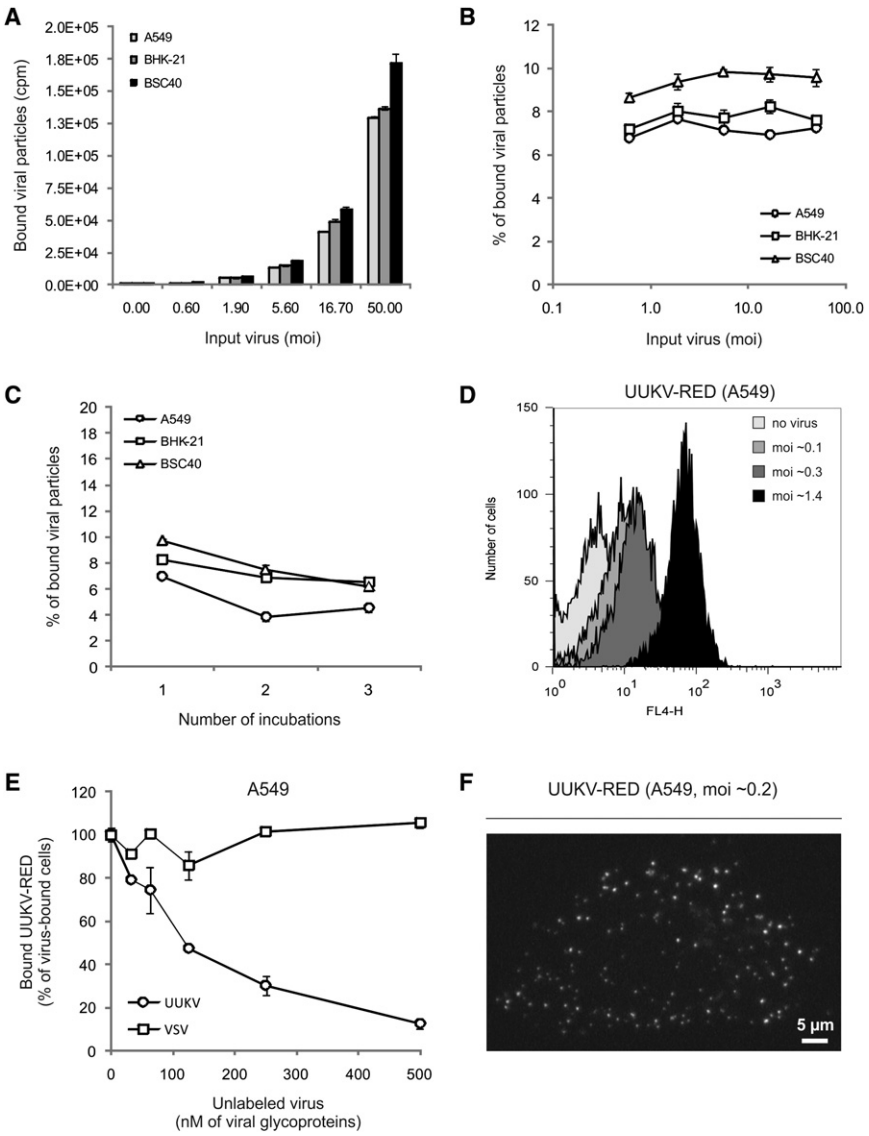

Figure 1. UUKV Binding to Cells Is Inefficient

(A) Serial dilutions of ^{35}S-labeled UUKV were bound to cells and samples quantified using a scintillation counter. Error bars indicate SD.

(B) Shows the same data as in (A) but expressed as the percentage of input virus bound to the cells (100 × bound particles [cpm]/input particles [cpm]). Error bars indicate SD.

(C) Supernatants from a previous binding experiment were added to new cells. This procedure was repeated three times. Data are expressed as in (B). Error bars indicate SD.

(D) Varying amounts of UUKV-RED were bound to cells and samples analyzed by flow cytometry.

(E) Shows a binding competition between unlabeled and fluorescent particles. Virus inputs were normalized according to the concentration of viral glycoproteins. Cells were preincubated with varying amounts of unlabeled particles (UUKV or VSV) and then exposed to UUKV-RED (2.5 nM) as described in (D). Error bars indicate SD.

(F) UUKV-RED was bound to cells on ice and samples analyzed with confocal microscope. White spots are cell-associated virus particles seen in a series of z stacks merged to one plane.

found that ten were infected and four produced virus (Table S1). For our study, we selected three of the productive cell lines representing human, rodent, and monkey cells (A549, BHK-21, and BSC40, respectively). In A549 and BSC40 cells, a complete cycle took about 12 hr, i.e., somewhat longer than in BHK-21 cells (data not shown). The two mosquito-derived lines tested were not infected.

Labeling of UUKV with ^{35}S-Amino Acids or Fluorescent Dyes

To quantify and visualize early stages of UUKV entry, we utilized purified virus labeled chemically with a fluorescent probe or radioactively using [^{35}S] cysteine and methionine in the cell culture medium. To render the virus fluorescent, we took advantage of the presence of exposed free cysteines in the glycoproteins G_N and G_C, to which we coupled a thiosulfate-activated fluorescent dye (TS-link Bodipy-TR) (UUKV-RED). The characterization of the fluorescently and radiolabeled particles is shown in Figure S2. The purity of the labeled UUKV preparations was greater than 90%. In the radioactive virus, the ^{35}S label was present in N, G_N, and G_C, whereas G_N and G_C were the only fluorescently labeled proteins in the UUKV-RED preparation (Figures S2A and S2B). That the nucleoprotein N was not fluorescent indicated that the viral envelope was intact. The different labeled particles could be visualized as single spots by confocal fluorescence microscopy and as 132 nm particles by EM after negative staining (Figures S2C–S2E). We noticed no significant impact of labeling on UUKV infectivity; the titers were similar to those of nonlabeled particles (Figure S2F).

UUKV Cell Binding Is Specific but Inefficient

To analyze binding to cells, increasing amounts of ^{35}S-labeled UUKV were first allowed to bind to cells on ice for 2 hr (moi of 0.6–50). The unbound viruses were washed away and remaining cell-associated radioactivity determined by scintillation counting. The results showed that binding increased with increasing concentration of input UUKV (Figure 1A), but with all three cell lines the fraction that associated with the cells was 7%–9% (Figure 1B). When the supernatant from a binding experiment was added to new cells, the fraction of radioactivity bound was similar, suggesting that the unbound virus was fully capable of cell association (Figure 1C). This indicated that the binding of UUKV to its host cells was inefficient.

The FACS assay allowed detection of the UUKV-RED bound from moi of 0.1 upwards (Figure 1D). Binding of UUKV-RED was found to be abolished by prebinding of unlabeled UUKV in

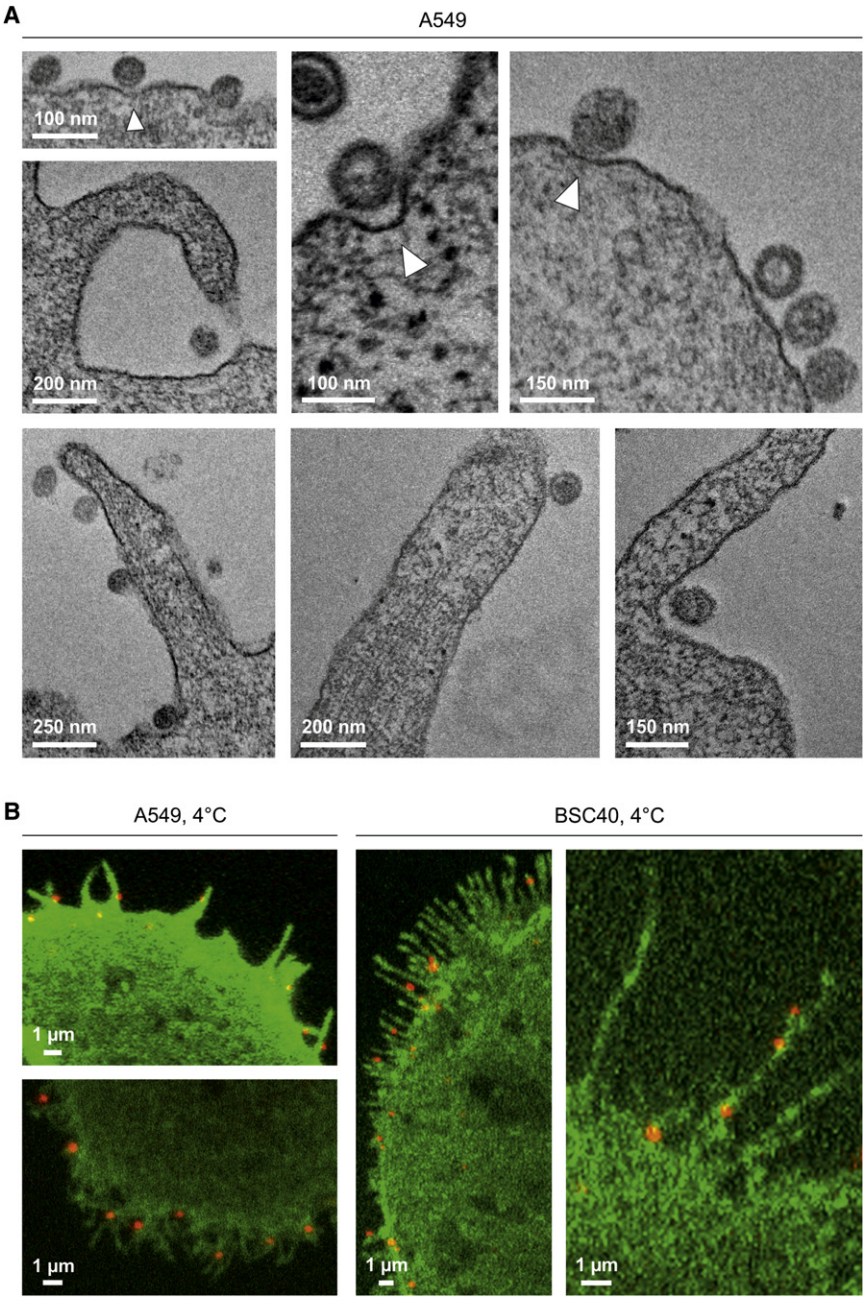

Figure 2. UUKV Binds to Filopodia

(A) EM of UUKV associated with the plasma membrane. The cells were exposed to the virus and analyzed in thin sections. Some of the membrane-bound viruses were associated with invaginations (white arrowheads).

(B) UUKV-RED (moi ~1) was bound to cells expressing PH-PLCΔ1EGFP and samples analyzed by confocal microscopy. Pictures show UUKV-RED association with filopodia.

a dose-dependent manner (Figure 1E). A 50-fold higher concentration of unlabeled particles reduced UUKV-RED binding to half, and a 200-fold higher concentration to 10%. Prebinding of vesicular stomatitis virus (VSV) did not affect UUKV-RED binding (Figure 1E). Taken together, these experiments indicate that UUKV binds rather inefficiently to cells, but binding most likely involves one or more specific attachment factors or receptors.

After binding of UUKV-RED at 4°C to A549, individual virus particles could be seen on the cell surface by confocal microscopy (Figure 1F). That the number of spots per cell was more than a hundred at a multiplicity of infection (moi) of only 0.2 indicated that the ratio between infectious and noninfectious particles was low.

Thin-section EM showed that UUKV bound to the A549 cell surface occurred as single particles with a distance of 11.4 ± 2.8 nm (n = 30) between the viral and the plasma membranes (Figure 2A). Some could be seen within shallow plasma membrane indentations that lacked a visible cytoplasmic coat (Figure 2A, white arrowheads). About half were associated with filopodia or located at their base (47 of 96 particles analyzed).

Fluorescence microscopy of cells expressing a fluorescent protein marker in the plasma membrane (PH-PLCΔ1 conjugated to the enhanced green fluorescent protein [EGFP]) confirmed the association of UUKV-RED with filopodia (Figure 2B). Note that filopodia in A549 and BSC40 cells differed in length and shape.

UUKV Internalization Is Mainly Clathrin Independent

To analyze UUKV internalization by fluorescence microscopy, we first allowed UUKV-RED to bind to BSC40 cells on ice at a relatively high moi (~7.5), and then the cells were warmed in the presence of ammonium chloride (NH_4Cl) to prevent penetration. After 40 min, the cells were placed back on ice to stop further endocytosis. To distinguish between internalized and surface-bound particles, the cells were treated with tris(2-carboxyethyl)phosphine (TCEP) for 30 min on ice. Since TCEP is a membrane-impermeable reducing agent, it only removed the dye from UUKV-RED still exposed at the plasma membrane. In samples treated with TCEP before warming, we observed little background fluorescence (Figure 3A [4°C, +TCEP]), whereas after warming internalized viruses could be seen as fluorescent spots of different intensities within the cells (Figure 3A [37°C, +TCEP]). We estimated that 25% of the cell-bound particles were internalized within 40 min.

To determine the kinetics of uptake, a more quantitative assay was used. Cells were incubated on ice with ^{35}S-labeled particles. After washing, the cells were treated with trypsin on ice to remove the surface-bound virus. Of cell-associated radioactivity

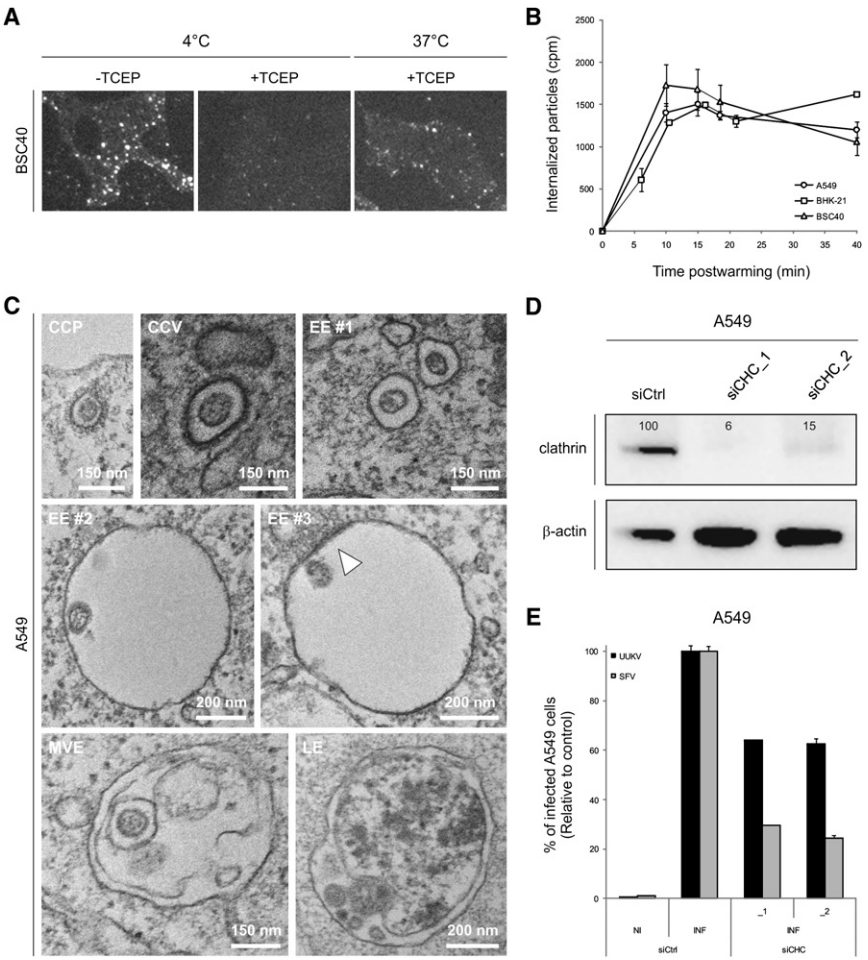

Figure 3. UUKV Entry Is Mainly Clathrin Independent

(A) UUKV-RED (moi ~7.5) was bound to cells and then samples shifted to 37°C in the presence of NH_4Cl (50 mM) for 40 min to allow internalization. Cells were subsequently treated with TCEP (a membrane-impermeable reducing agent) to distinguish internalized from external particles and analyzed by wide-field microscopy.

(B) Internalization time course of ^{35}S-labeled UUKV (moi ~3). The fraction that could not be removed by trypsin treatment was considered as background and subtracted from other values. Error bars indicate SD.

(C) Cells were exposed to UUKV on ice and subsequently warmed rapidly to 37°C to allow internalization. Using EM, viruses were very rarely seen in CCP and CCV but often in small, uncoated vesicles (EE #1). UUKV was also observed in larger endosomal structures (EE #2 and #3). These vacuoles were sometimes associated with electron-dense structures on their cytosolic surfaces (EE #3, white arrowhead). At later stages, viruses were often found in MVE and in structures which could correspond to LE or autophagic vesicles.

(D) Efficiency of CHC knockdown assayed by western blotting. CHC protein levels are expressed as percentages of CHC levels in cells treated with CHC siRNAs (siCHC_1 and _2) normalized to levels of β-actin and CHC in control cells treated with negative-control siRNA (siCtrl).

(E) Cells treated with CHC siRNAs were infected with UUKV or SFV. The values were normalized to the number of cells and the infection level in samples treated with negative-control siRNA (siCtrl). NI and INF for noninfected and infected cells, respectively. Error bars indicate SD.

after binding in the cold, more than 90% was removed by this procedure (Figure S3). In contrast, if the cells were warmed to 37°C for 20 min prior to trypsin treatment, about one-third of the ^{35}S-labeled particles became inaccessible to trypsin (Figure S3). When the generation of trypsin-resistant virus was analyzed over time, it was found that the maximum level of internalization was reached already within 10 min (Figure 3B). Taking into account the background, we could confirm that 25% of cell-bound particles were rapidly endocytosed.

To assess internalization using EM, cells were exposed to virus at high moi on ice and rapidly shifted to 37°C to allow internalization. After 2 min, viruses were seen in smooth-surfaced vesicles with a diameter of about 150 nm often located close to the plasma membrane (Figure 3C, EE #1). In rare cases, viruses could be seen to associate with clathrin-coated pits (CCPs) and vesicles (CCVs) (Figure 3C). After 10 min, UUKV was observed in classical endosomal vacuoles with diameters of 400–500 nm (Figure 3C, EE #2 and #3). Some of these bore electron-dense structures on their cytosolic surface (EE #3), characteristic of protein clusters containing clathrin and the endosomal sorting complex required for transport (ESCRT) complexes, and typical of early endosomes (EEs) (Sachse et al., 2002). After 30 min, viruses were often found in multivesicular endosomes (MVEs) and in vacuoles that could represent late endosomes (LEs) (Figure 3C, MVE and LE). Virus fusion with the limiting membrane or intraluminal vesicles was not observed.

To further address the potential involvement of CME in infection, we depleted A549 cells of clathrin heavy chain (CHC) using two different, nonoverlapping small interfering RNAs (siRNAs) in parallel experiments. With each siRNA, the level of CHC protein in the cultures was reduced by 85%–95% as assayed by western blotting (Figure 3D). The CHC siRNA-treated cells were still efficiently infected by UUKV. The decrease in infection was only 35% for both CHC siRNAs compared to the control cells transfected with a control siRNA (Figure 3E). As a control for assessing the effectiveness of CHC knockdown, we used Semliki Forest virus (SFV), which exclusively uses the clathrin pathway (Doxsey et al., 1987). In contrast to UUKV, infection with SFV was strongly inhibited in these cells, with a 75%–80% decrease in comparison to the control (Figure 3E). Taken together, the results suggest that although some viral particles could be seen in CCP and CCV, the majority are endocytosed by mechanisms that do not involve clathrin coats.

UUKV Enters EE and LE

The EM studies suggest that the internalized viruses were transported to endosomes. To better define the endocytic route taken

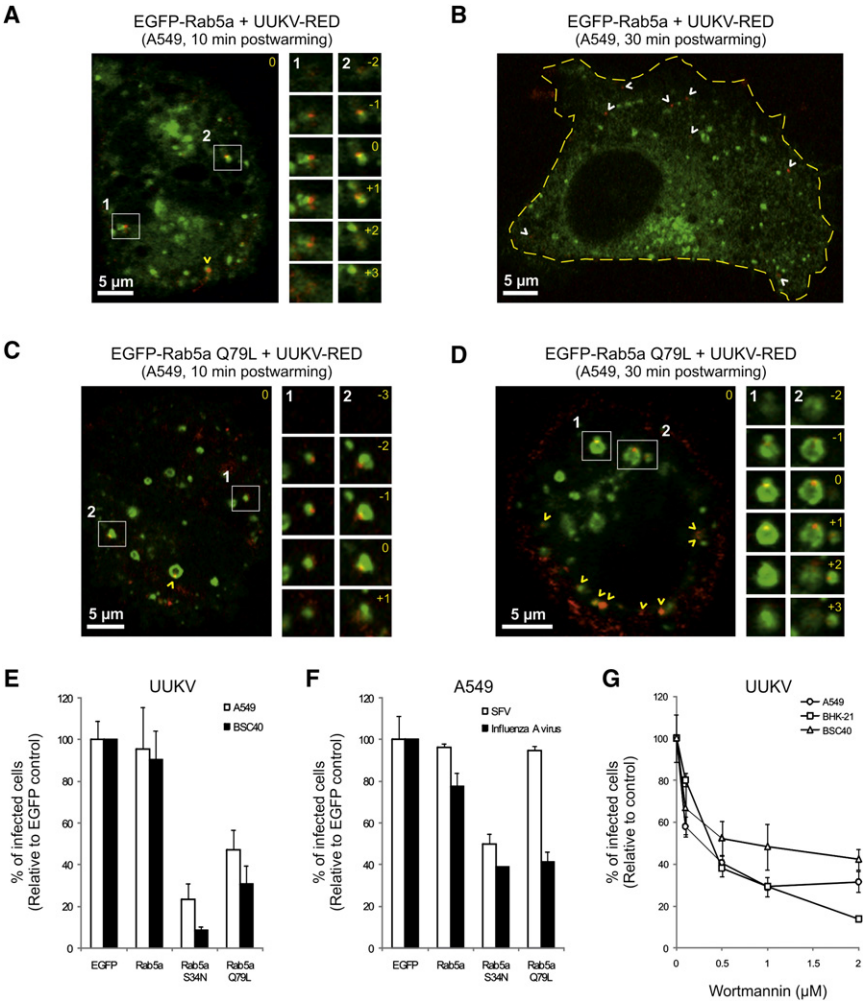

Figure 4. UUKV Enters Endocytic Machinery through Rab5a-Positive EE

(A–D) Entry of prebound UUKV-RED (moi ~10) into cells expressing EGFP-Rab5a (A and B) or EGFP-Rab5a Q79L (C and D) by confocal microscopy. Viruses were internalized for 10 min (A and C) or 30 min (B and D) at 37°C. One focal plane is shown. UUKV is seen in red and EE containing EGFP-Rab5a or Q79L in green. Higher magnifications of association between UUKV and Rab5a-positive vesicles (white numbers and squares) are shown on the right borders as a z stack series. Yellow numbers indicate the position of the stack in the series compared with the original plane marked 0. White and yellow arrowheads show nonlocalizing and colocalizing, internalized particles, respectively. The yellow dotted line delimits the plasma membrane.

(E) EGFP-Rab5a WT, S34N, and Q79L were transiently expressed in cells. The cells were then infected with UUKV at a moi of 2. Using FACS, one population of cells was selected 7 hr postinfection in each sample based on intensity range of the EGFP signal. From this population, infection was quantified and normalized to EGFP-expressing cells. Error bars indicate SD.

(F) Effect of EGFP-Rab5a WT, S34N, and Q79L expression on SFV and influenza A virus infection. Quantification was performed as described in (E). Error bars indicate SD.

(G) Cells were pretreated with wortmannin and infected with UUKV. Data are normalized to samples where the inhibitor had been omitted. Error bars indicate SD.

by this virus, we determined next whether the viruses reached EE. After binding of UUKV-RED (moi ~10) on ice to A549 cells expressing the EE marker Rab5a tagged with EGFP (EGFP-Rab5a), the temperature was rapidly shifted to 37°C for periods of up to 30 min. Confocal microscopy showed UUKV colocalizing with EGFP-Rab5a in cytoplasmic vesicles 5 min postwarming (data not shown). The amount of colocalizing virus reached a maximum 10 min postwarming and decreased thereafter until no longer detectable after a further 30 min (Figures 4A and 4B). In live BSC40 cells, spinning-disc confocal microscopy showed that UUKV-RED actually moved in the cytoplasm with the EGFP-Rab5a-positive vesicles (Movie S1).

Colocalization of UUKV with vacuoles containing the LE and lysosome markers Rab7a and LAMP-1 (EGFP-Rab7a and EGFP-LAMP-1) was also observed, but at later time points. Colocalization and coordinated movement with EGFP-Rab7a in live cells occurred 20–30 min after warming (Figure 7A and Movie S2). Colocalization with EGFP-LAMP-1 was maximal between 30 and 40 min (Figure 7B), and coordinated motion was also observed (Movie S3). At this time the majority of internalized particles were associated with EGFP-LAMP-1-positive vesicles. Note that some particles were localized in the middle of the vesicles, suggesting that the viruses had not yet undergone fusion with the limiting membrane (Figure 7B).

Passage through EE and Infectivity

To determine whether passage through the endosomal compartments was required for infectivity, we first assessed UUKV internalization and infection in cells expressing a constitutively active mutant of Rab5a (EGFP-Rab5a Q79L). Expression of this mutant results in enlargement of EE, as seen in Figures 4C and 4D (Stenmark et al., 1994). Maturation of LE and transport of cargo to lysosomes are compromised (Hirota et al., 2007; Rosenfeld et al., 2001). In A549 and BSC40 cells expressing EGFP-Rab5a Q79L, we found that UUKV infection was reduced by 50%–70% compared with cells expressing EGFP-Rab5a wild-type or EGFP only (Figure 4E). In contrast to EGFP-Rab5a, the number of viruses colocalizing with EGFP-Rab5a Q79L-positive vesicles was significantly elevated even after 30 min (Figures 4C and 4D). At this time, virtually all internalized particles were associated with the giant EE, consistent with a block in transport to LE and lysosomes.

Wortmannin, an inhibitor of phosphoinositide (PI)3-kinase (an important effector of Rab5a), has been shown to induce the

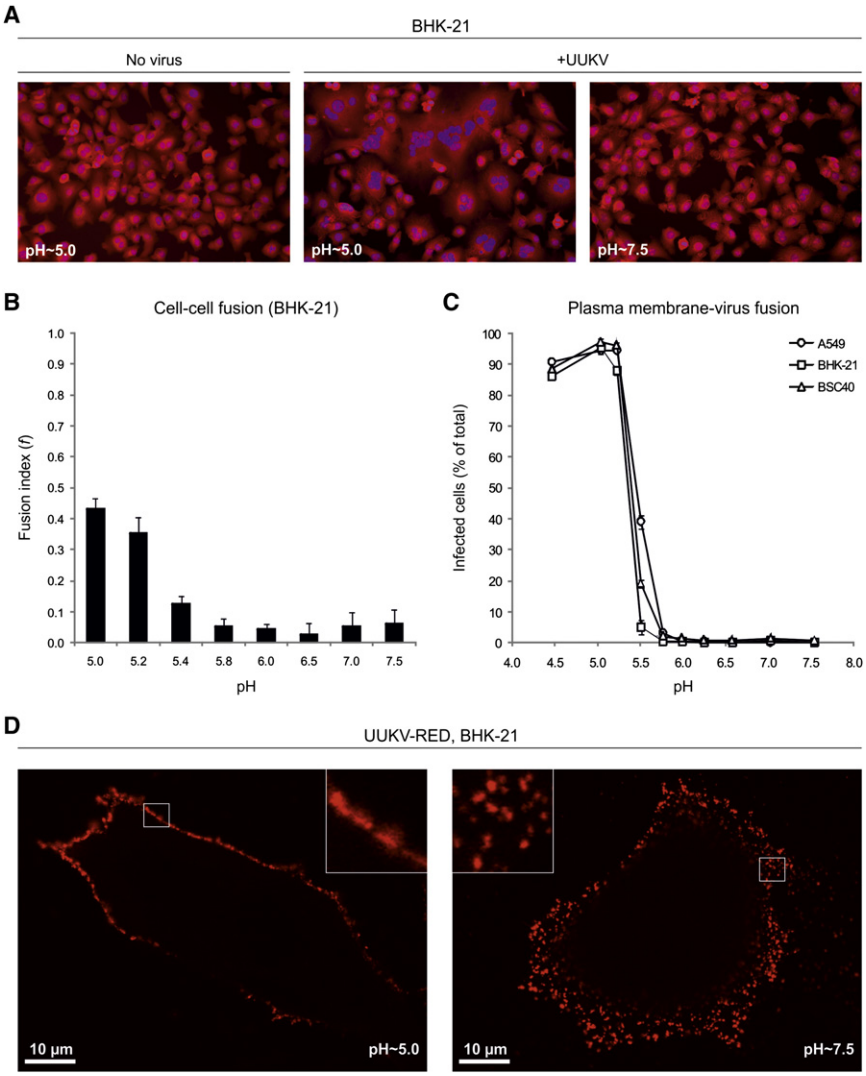

Figure 5. The pH Threshold for UUKV Membrane Fusion Is 5.4

(A) Confluent monolayer of cells was exposed to UUKV (moi ~1000) on ice and then treated for 5 min at 37°C with buffers at indicated pH. Nuclei and cytoplasm were stained 3 hr postwarming with bisbenzimide and CellMask Deep Red, respectively.

(B) Shows the quantification of data obtained in (A). Fusion index is given as $f = (1 - [c/n])$, where c is the number of cells in a field after fusion and n the number of nuclei. Error bars indicate SD.

(C) Confluent monolayers of cells were exposed to UUKV (moi ~5–30) on ice, treated with varying pH for 1.5 min at 37°C, and then incubated for up to 18 hr at 37°C in the presence of NH_4Cl (50 mM) to block further penetration from endocytic vesicles. The infection was determined by FACS. Error bars indicate SD.

(D) Shows the fusion of UUKV-RED (moi ~2) with the plasma membrane in one confocal plane using the protocol described in (C). Higher magnifications of the plasma membrane are shown in the corners (white squares).

formation of similar, enlarged early endocytic vesicles (Houle and Marceau, 2003). When cells were pretreated with wortmannin, infection was also efficiently inhibited (Figure 4G).

Expression of a dominant-active mutant of Rab5a (EGFP-Rab5a S34N), which abrogates the maturation of newly formed EE (Stenmark et al., 1994), also resulted in a strong decrease in infection (80%–90%) in both cell lines (Figure 4E). Similar results were observed for influenza A virus, another late-penetrating virus (Figure 4F). Interestingly, Rab5a S34N, and not Rab5a Q79L, reduced SFV infection, indicating that a virus with a fusion threshold between pH 6.0 and 6.2 can fuse in giant Rab5a Q79L-positive EE, whereas UUKV and influenza A virus cannot (Figures 4E and 4F). Altogether, these results showed that the infectious entry pathway involves passage through Rab5a-positive endosomes, but transport to downstream organelles is also needed for productive infection.

Low pH Dependence of UUKV Infectious Entry

To test whether the acidic pH in endosomal vacuoles was important in UUKV infection, virus was added to cells in the presence of agents that neutralize vacuolar pH. The lysomotropic weak bases NH_4Cl and chloroquine induced a dose-dependent inhibition of UUKV infection in all three cell lines (Figure S4A). In these experiments, we made certain that the pH in the medium did not drop below pH ~7.0 to ensure the effectiveness of the drugs (Mercer et al., 2010).

Two inhibitors of vacuolar-type H^+-ATPases (vATPases), bafilomycin A1 and concanamycin B, gave similar results (Figure S4B). The drugs were dissolved in ethanol or methanol, which unlike dimethyl sulfoxide had no adverse effects on infection (Figure S5). We confirmed the involvement of the vATPase using four different siRNAs to deplete the V1 subunit A (vATPV1A) of these proton pumps. The level of vATPV1A protein was reduced by 85%–95% as assayed by western blotting (Figure S4C). The silencing led to a strong inhibition of UUKV infection (from 75% to 95%) (Figure S4D). Together, these results demonstrate that UUKV infection depends upon vacuolar acidification.

Low pH Is Sufficient and Necessary for UUKV Fusion

To determine whether the acid-induced step involved membrane fusion, we assessed the capacity of UUKV to mediate cell-cell fusion (“fusion-from-without”) as previously described for other enveloped viruses (White et al., 1981). Briefly, large amounts of virus were allowed to bind to confluent BHK-21 cells in the cold, and the cells were warmed using buffers of different pH. When the pH of the buffers was 5.4 or below, the formation of syncitia with five or more nuclei was observed (Figure 5A).

The extent of cell-cell fusion was determined using a fusion index that expresses the average number of fusion events per

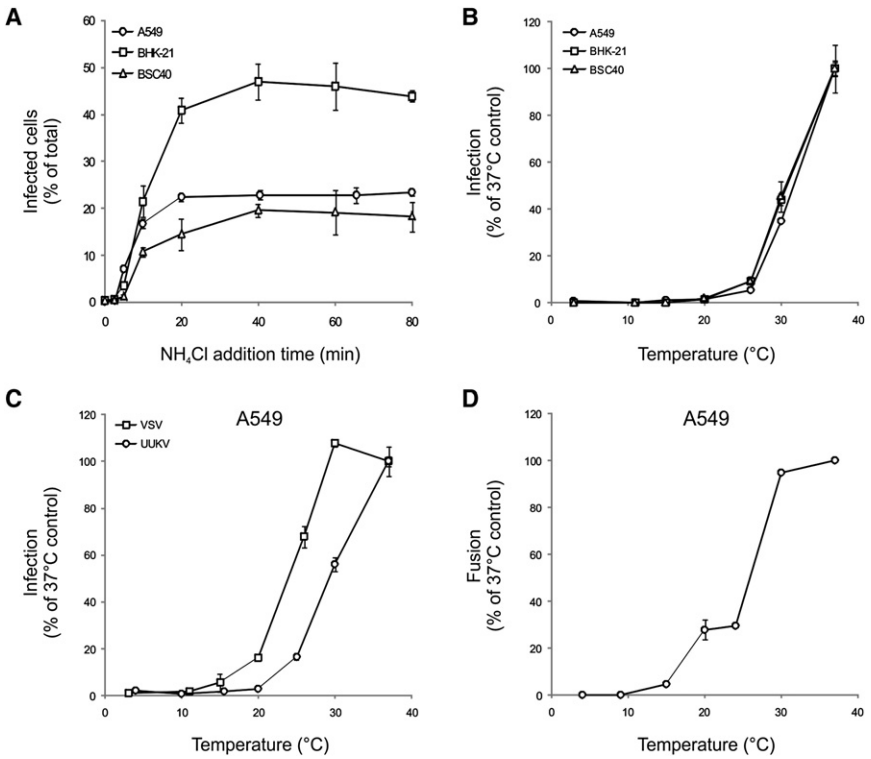

Figure 6. The UUKV Acid-Activated Penetration Occurs within 40 Min after internalization and Is Temperature Dependent

(A) Cells were exposed to UUKV on ice and then shifted to 37°C to allow internalization. NH_4Cl was added at different times to block further penetration. Error bars indicate SD.

(B) UUKV was bound to cells on ice and samples shifted to different temperatures for 1 hr. Infected cells were then incubated at 37°C in the presence of NH_4Cl to block further penetration. Error bars indicate SD.

(C) As a prototype virus entering through EE, VSV was used in the infection assay described in (B) and compared to UUKV for the temperature dependence. Error bars indicate SD.

(D) UUKV fusion efficiency was assessed at the indicated temperatures using the plasma membrane-virus fusion assay described in Figure 5C. Error bars indicate SD.

original mononucleated cell (Figure 5B) (White et al., 1981). The index reaches 1 when all of the nuclei in the microscope field are present in a single cell, and the value is 0 when all cells have one nucleus each. The fusion index with BHK-21 cells of 0.4 was reached at pH ~5.2 and below (Figure 5B).

To define more accurately the pH threshold and to link fusion with infection, we assessed the capacity of UUKV to fuse with the plasma membrane of cells and thus bypass the need for endocytosis during productive infection, as previously described for SFV (Helenius et al., 1980). Briefly, UUKV was allowed to bind to cells on ice, the temperature was rapidly shifted to 37°C for 1.5 min in buffers with different pHs, and NH_4Cl-containing medium at neutral pH added for the remaining infection period to prevent infection via endosomes. To confirm that the addition of NH_4Cl prevented infection through endocytosed viruses after the low-pH treatment of cells, cells were treated first at pH ~4.5 and then exposed to UUKV in the presence of NH_4Cl. Low pH-treated cells were infected as efficiently as mock-treated cells, and NH_4Cl completely inhibited infection under both conditions (Figure S6).

As shown in Figure 5C, the bypass resulted in efficient infection. The level of infection was actually doubled compared to normal infection with the same amount of virus bound (data not shown). The reason was probably the inefficient endocytosis of the virus. Interestingly, raji cells, which are normally not infected, were infected when the bypass protocol was used. At moi of 10, 70% of the raji cells could be infected by fusing the viruses with the plasma membrane. In A549 and BSC40 cells, the bypass worked at pH values of 5.8 and below, while in BHK-21 cells the pH needed was slightly lower. Fifty percent of maximal infection was reached at pH ~5.4 in all cell lines (Figure 5C).

The results indicate that a reduction in pH is sufficient to trigger fusion and infectious penetration of viral RNP through the plasma membrane into the cytosol. Additional processing steps in the endosomal compartments were apparently not required to activate fusion or infection by this virus. The bypass involved fusion of the viral membrane, and the plasma membrane was shown by the diffusion of the fluorescently labeled glycoproteins G_N and G_C into the plasma membrane of BHK-21 cells after acidification (Figure 5D). In contrast, under neutral pH conditions the fluorescent glycoproteins remained focal spots at the cell surface. The high density of viruses bound to the plasma membrane observed was due to use of a relatively high moi (~2).

Acid-Activated Penetration in Late Endosomal Compartments

To determine the timing of the acid-requiring step after endocytic entry, we took advantage of the fact that the elevation in endosomal pH is almost instantaneous when NH_4Cl is added to the extracellular medium (Ohkuma and Poole, 1978). After binding viruses at low moi (~1) in the cold, A549 cells were rapidly shifted to 37°C and NH_4Cl added at different times postwarming. It was apparent that infectious penetration started after a 5 min lag and reached a half-maximal level within 12 min in all three cell lines (Figure 6A). Evidently, exposure of individual viruses to a pH ~5.4 or lower occurred nonsynchronously during a time span 5–30 min after endocytic uptake.

The time course suggested that penetration might occur in LE. To pursue this possibility, we determined the temperature dependence of entry, because it is known that the transport of cargo from EE to LE is inhibited at temperatures below 20°C (Dunn et al., 1980). After binding of UUKV in the cold, cells were rapidly shifted to different temperatures for 1 hr. After addition of NH_4Cl to prevent further penetration, the cells were then

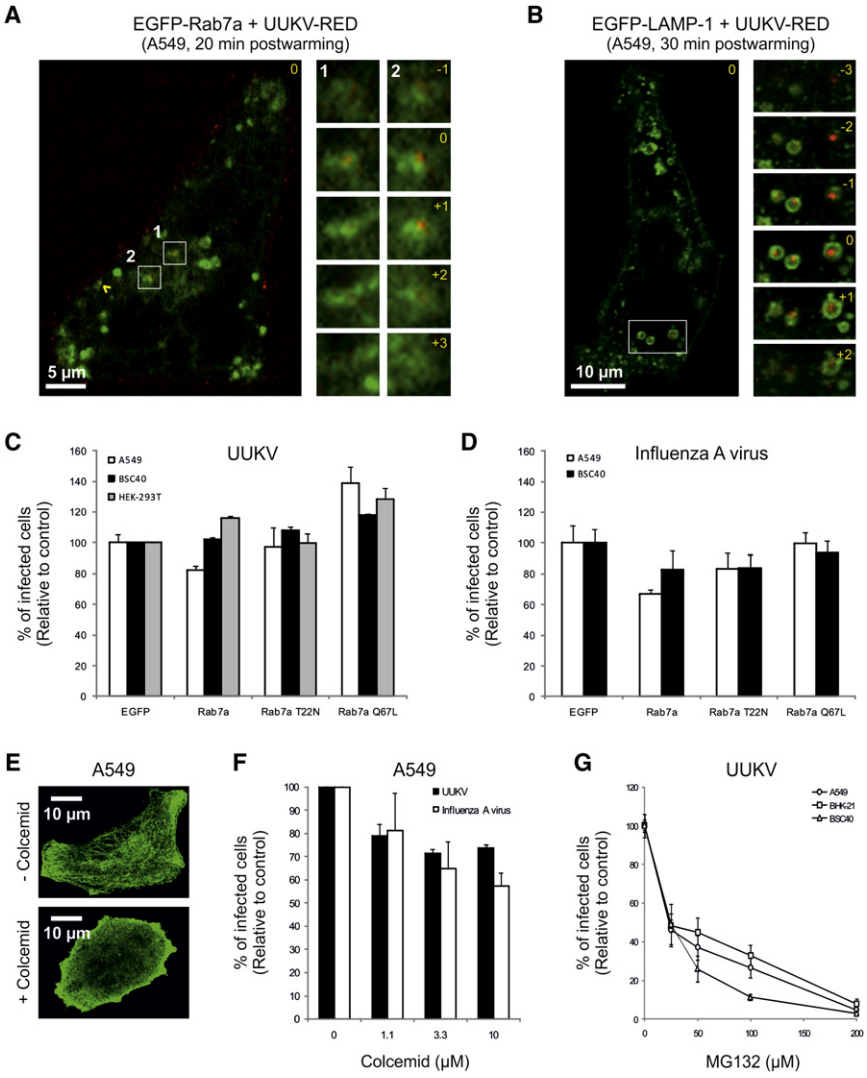

Figure 7. UUKV Enters in Late Endosomal Organelles

(A and B) Entry of prebound UUKV-RED (moi ~10) into cells expressing EGFP-Rab7a (A) or EGFP-LAMP-1 (B) by confocal microscopy. Viruses were internalized for 20 min (A) or 30 min (B) at 37°C. One focal plane is shown. UUKV is seen in red and LE containing EGFP-Rab7a or EGFP-LAMP-1 in green. Higher magnifications of association between UUKV and Rab7a- or LAMP-1-positive vesicles (white numbers and squares) are shown on the right borders as a z stack series. Yellow numbers indicate the position of the stack in the series compared with the original plane marked 0. Yellow arrowhead shows colocalizing particles.

(C and D) Effect of EGFP-Rab7a WT, T22N, and Q67L expression on UUKV and influenza A virus infection. Infection and quantification were performed as described in Figure 4E. Error bars indicate SD.

(E) Cells were treated with colcemid (10 μM) during 3 hr on ice, then stained with anti-α-tubulin antibody and analyzed by confocal microscopy.

(F and G) Cells were pretreated with colcemid or MG132 and then infected with UUKV or influenza A virus. Data are normalized to samples where the inhibitor had been omitted. Error bars indicate SD.

incubated at 37°C for the rest of the infection period. The expression of protein N was strongly inhibited in all three cell lines at 25°C and below (Figure 6B). In contrast to UUKV, infection by VSV, a virus that is acid activated in EE (Johannsdottir et al., 2009), was detected at temperatures as low as 15°C–20°C (Figure 5C).

To check whether the fusion process as such was affected by temperature, we assessed the temperature dependence of UUKV fusion using the bypass protocol (see above). At 30°C, fusion was as efficient as at 37°C, whereas infection was lowered by half (Figures 6B–6D). At 20°C, fusion was still almost 30% of the 37°C control, whereas infection via the normal route could no longer be detected (Figures 6B–3D). As expected of a virus capable of replicating in insect hosts, this suggested that fusion was not a bottleneck for penetration at lower temperatures. Most likely the viruses did not infect at 20°C and below because they did not reach a compartment with low enough pH.

Rab7a is a major organizer of LE maturation and function (Zhang et al., 2009). To assess its role in UUKV infection, we infected cells expressing dominant-negative or constitutively active mutants (EGFP-Rab7a T22N or EGFP-Rab7a Q67L, respectively). In A549 and BSC40 cells, expression of EGFP-Rab7a T22N did not block UUKV infection but also did not block infection by influenza A virus (Figures 7C and 7D). In contrast to influenza A virus, EGFP-Rab7a Q67L, however, promoted UUKV infection, by up to 40%, in all lines (Figure 7C).

In some cell types, the maturation of LE also depends on microtubule-mediated transport of endosomes to the perinuclear region of the cell (reviewed in Mercer et al., 2010) and on proteasome activity (Khor et al., 2003). For UUKV and influenza A virus, colcemid treatment resulted in a 30%–40% decrease in infection (Figures 7E and 7F). MG132, a proteasome inhibitor known to divert influenza A virus away from late endosomes (Khor et al., 2003), reduced UUKV infection in a dose-dependent manner in all three cell lines (Figure 7G). Altogether, these data show that UUKV resembles influenza A virus in that its entry depends on a normal maturation of LE. It is transported from EE to LE, and its pH of fusion corresponds to that prevailing in LE. It cannot infect cells in which cargo transport into the degradative branch of endocytic pathway is blocked.

DISCUSSION

In this study, we developed reliable and accurate assays to study UUKV infection, endocytosis, and membrane fusion in animal host cells, and applied fluorescence microscopy to track

UUKV during various stages of its entry program. To label the particles with thiosulfate-activated fluorescent dye or with [^{35}S] cysteine and methionine, we took advantage of the exceptionally large number of cysteines and methionines (55 and 19, respectively) in the UUKV glycoproteins, typical for bunyaviruses.

Regardless of the cell line used, binding of UUKV to the cell surface was specific but inefficient. EM and fluorescence microscopy showed preferential association with filopodia and with the region of the plasma membrane close to the filopodia base. Such interactions could be of importance in vivo since, for instance, dendritic cells, which are permissive to some bunyaviruses, have numerous dendrites and filopodia (Connolly-Andersen et al., 2009). EM showed that a space of about 11 nm separated the plasma membrane from the membrane of the viral particles, consistent with a recent cryo-EM study showing that the spike glycoproteins project between 10 and 15 nm from the virus envelope (Overby et al., 2008). The identity of UUKV receptors remains to be determined.

After binding, internalization of viruses occurred. It involved about one-quarter of the surface-bound particles, amounting to less than 2% of total input virus. Although inefficient, it was rapid; the endocytosis phase was completed within 10 min. The reason why so many of the bound viruses failed to enter is unclear, but similar observations have been made for other viruses such as VSV (Johannsdottir et al., 2009).

CME has been reported to be critical for entry of some orthobunya-, nairo-, and hantaviruses (Jin et al., 2002; Santos et al., 2008; Simon et al., 2009b). By EM, we could observe some of the UUKV particles in CCP and CCV, but these were rare. The majority were located in noncoated indentations at the plasma membrane and after endocytosis in noncoated, small cytoplasmic vesicles. The vesicles could represent CCV that had lost their clathrin coat or primary vesicles in a clathrin-independent pathway. The marginal effect of CHC knockdown compared to SFV could reflect the diversity of endocytic pathways used by UUKV or also differences in the role of clathrin in other processes, such as receptor recycling. Together, the results suggested that the majority of UUKV particles use a clathrin-independent pathway for infectious entry. After endocytic uptake, viruses were observed in larger vesicles, with the morphology of EE, LE, and MVE indicating that after internalization the viruses were channeled into the classical endosome pathway.

The penetration of enveloped viruses involves fusion between the viral envelope and a cell membrane. In the majority of cases, fusion is triggered in endosomes after acid activation of viral glycoproteins (Mercer et al., 2010). The first indication that UUKV shares this penetration strategy was the sensitivity of infection to agents that elevate vacuolar pH. Using NH_4Cl, we showed that the first viruses reached the acid-dependent step 5 min after cell warming, and that half of the incoming, infectious particles passed the NH_4Cl-sensitive step within 12 min. The time course resembled that of other viruses penetrating from LE, such as lymphocytic choriomeningitis virus (LCMV), influenza A, and minor rhinoviruses (Martin and Helenius, 1991; Prchla et al., 1994; Quirin et al., 2008). These viruses pass the acid-sensitive step typically with a half-time of 10–20 min. For comparison, viruses fusing in EE, such as VSV or SFV, become NH_4Cl insensitive within 5 min as their uptake is almost instantaneously followed by acid activation (Johannsdottir et al., 2009; Quirin et al., 2008).

That UUKV does indeed possess acid-triggered membrane fusion activity was demonstrated in two ways: the induction of cell-cell fusion by externally added virus particles (“fusion-from-without”), and the fusion of bound viruses to the plasma membrane of cells. In both cases, fusion was triggered at pH below 5.8 with an optimum at 5.4. These are relatively low pH values; i.e., comparable to influenza A virus and thus consistent with penetration in LE. By forcing the glycoproteins of other bunyaviruses to the cell surface through overexpression, others have measured cell-cell fusion “from within” and found that formation of syncitia occurred at slightly higher pH values, namely 5.8–6.4 with a threshold of about 6.0 (Filone et al., 2006; Plassmeyer et al., 2007). Exactly what happens to glycoproteins G_N and G_C upon acidification is unclear. It has been reported that their biochemical properties undergo a change (Overby et al., 2008; Ronka et al., 1995). Computational modeling based on the known structures of glycoproteins of other arboviruses, such as *Flavivirus* or *Alphavirus*, suggest that G_C could be responsible for *Orthobunyavirus* and *Hantavirus* fusion (Garry and Garry, 2004; Tischler et al., 2005).

The UUKV-mediated cell-cell and virus-cell fusion demonstrated that low pH is sufficient to trigger fusion. Proteolytic processing in endosomes as observed for Ebola virus was apparently not needed (Kaletsky et al., 2007). The results also indicated that the RNP could be released directly through the plasma membrane into the cytosol in infectious form. Acid activation occurred in less than 1.5 min, consistent with pH-triggered kinetics observed for other acid-dependent viruses (Wessels et al., 2007). More functional investigations will be required to determine whether receptors play a role in UUKV fusion.

It is clear from our data that, like SFV and influenza A virus, UUKV depends on endocytosis and membrane transport within the classical endosomal system for infection. Expression of Rab5a S34N, which inhibits maturation of EE and homotypic EE fusion, affected all three viruses. In contrast, Rab5a Q79L and wortmannin, which cause expansion of EE and prevent proper LE maturation, only affected the late-penetrating viruses influenza A virus and UUKV. Similar observations have been recently reported for parvoviruses and for human rhinovirus serotype 2 (HRV2), which are late penetrating (Brabec et al., 2006; Harbison et al., 2009). That Rab5a Q79L had no adverse effect on SFV infection suggested that the pH in the giant EE was low enough to mediate fusion of this early-penetrating virus. One can conclude that UUKV passes through Rab5a-positive EE, but to be infectious it must reach more acidic downstream organelles, most probably late endosomal compartments.

Other observations supported the notion that for UUKV the acid-activated step occurred in LE. One was the timing of the NH_4Cl-inhibited step (20–40 min), another one the inhibition of infection observed at temperatures below 25°C. More directly, fluorescence confocal microscopy showed that the arrival of particles in Rab7a- or LAMP-1-positive LE coincided roughly with the time of acid activation. The sensitivity to MG132, a proteasome inhibitor, mirrored observations with influenza A and murine coronaviruses, which accumulated in cytosolic vacuoles and failed to infect (Khor et al., 2003; Yu and Lai, 2005). Further

investigations will be required to determine the role of ubiquitination and the proteasome in the maturation of endosomes.

Like Rab5 for EE, it is known that Rab7 plays a critical role in the formation and function of late endocytic compartments (Zhang et al., 2009). It is a key regulator in LE maturation, endosome movement, and fusion with lysosomes. Expression of the constitutively active Rab7a construct increased UUKV infectivity significantly. However, given the many indications that UUKV entered LE and used them for penetration, it was surprising that the inactive mutant Rab7 T22N did not have a more dramatic effect on infection. However, expression of Rab7 T22N has also not been found to affect infection by other late-penetrating viruses such as LCMV (Quirin et al., 2008). There could be many explanations for this, such as the presence of multiple isoforms of Rab7, the lack of dominant-negative effect of the mutant, mislocalization of the mutant Rabs, etc. (Bucci et al., 2000). It is apparent that results using Rab7 perturbants need to be interpreted with caution, and that the perturbations of the endosomal pathway need to be carefully evaluated in various virus systems and cell lines.

Our results indicated that UUKV is a late-penetrating virus and as such a member of a group of viruses that seem to use LE and possibly endolysosomes for penetration or transit. They include influenza A virus, dengue virus serotype 2 strain 1, HRV2, LCMV, canine and feline parvoviruses, murine and simian 40 polyomaviruses, and human papillomavirus 16 (Brabec et al., 2006; Harbison et al., 2009; Mercer et al., 2010; Qian et al., 2009; Quirin et al., 2008; Sieczkarski and Whittaker, 2003; van der Schaar et al., 2008). Although they use diverse cell surface receptors, signaling pathways, and primary endocytic mechanisms, most of them seem to pass through EE, from which they are sorted into the degradative branch of the endocytic pathway. Penetration is not activated in EE. Instead they move together with endocytosed cargo and intralumenal vesicles into maturing endosomes, LE, endolysosomes, and lysosomes deeper into the cell. Typically, penetration occurs in the maturing endosomes or LE, but even later compartments cannot be excluded for some of them. The main distinction between these viruses and early-penetrating viruses such as SFV and VSV is that they have a lower pH threshold (5.4–5.8) of activation and therefore a longer half-time of penetration (>10–15 min) (Mercer et al., 2010). Viruses of the polyoma family are exceptions because they continue from late endosomal organelles to the endoplasmic reticulum where penetration occurs (Qian et al., 2009). Unlike early-penetrating viruses, late viruses are sensitive to treatments that inhibit the proper maturation of LE and cargo transport into the degradative branch of the endocytic pathway. With the results presented here, UUKV can be confidently classified as a member of this interesting group of viruses, the detailed cell biology of which remains a challenge for future work.

EXPERIMENTAL PROCEDURES

Cells and Viruses

All cell lines were cultured according to ATCC recommendations. All products used for cell culture were from Invitrogen. The prototype strain of UUKV S23 has been described previously (Pettersson and Kaariainen, 1973). Production, purification, titration, and labeling of viruses were performed as previously described elsewhere (Johannsdottir et al., 2009; Quirin et al., 2008). The moi is given according to the titer determined for each cell line.

Binding and Internalization Assays

Virus binding to cells was performed on ice as previously described (Johannsdottir et al., 2009). For competition with unlabeled viral particles, cells were preincubated for 30 min at 4°C with varying concentrations of unlabeled particles before addition of UUKV-RED. For internalization, the virus-bound cells were shifted rapidly to 37°C for up to 40 min before fixation. ^{35}S-labeled UUKV internalization was performed as previously described (Marsh and Helenius, 1980).

Electron Microscopy

Negative staining of samples containing UUKV-RED was performed with phosphotungstic acid at pH ~7.4 as previously described (von Bonsdorff and Pettersson, 1975). For thin-section EM, after exposure to virus (moi ~100), cells were fixed and treated as previously described (Johannsdottir et al., 2009).

Fluorescence Microscopy

For confocal microscopy, cells were transfected prior to exposure to UUKV-RED, then analyzed with a Zeiss LSM510 Meta microscope or a spinning-disc Visitech microscope. For live-cell imaging, analysis was performed in the presence of virus. For TCEP-based internalization assay, uptake of UUKV-RED was monitored with a Zeiss Axiovert microscope. To distinguish between internalized and external particles, samples were treated three times with 50 mM TCEP (Pierce, supplemented with 50 mM Tris-HCl [pH ~8.0], 125 mM NaCl, 50 mM HEPES, and 1 mM $MgCl_2$) for 10 min at 4°C, before fixation.

UUKV Infection Assay

Cells were exposed to UUKV (moi from 1 to 10) for 1 hr at 37°C. Viral supernatant was subsequently replaced by culture medium, and the cells were incubated at 37°C for indicated times (up to 18 hr). For all infection experiments, infected cells were quantified by flow cytometry as shown in Figure S1B and previously described (Quirin et al., 2008). For inhibition assays, cells were pretreated with drugs for 30 min at 37°C (except for colcemid, 3 hr on ice) and then exposed to UUKV (moi ~2) for 1 hr in the presence of the drugs. UUKV-exposed cells were subsequently incubated in culture medium supplemented with drugs for 6 hr at 37°C. Drugs were used at concentrations for which we did not observe any effect on cell viability. For siRNA-based infection assays, transfected cells were washed 1 hr before infection. For EGFP-Rabs-based infection assays, cells were transfected and washed 6 hr later. Transfected cells were exposed to the viruses 18 hr posttransfection.

Cell-Cell and Plasma Membrane-Virus Fusion Assays

Cell-cell and plasma membrane-virus fusion assays were performed as previously described (Helenius et al., 1980; White et al., 1981). For fusion of fluorescent particles at the plasma membrane (moi ~2), virus-bound cells were fixed in neutral pH conditions after low pH treatment and then analyzed by confocal microscopy as described above.

NH_4Cl Add-In Time Course

Virus binding (moi ~1) was synchronized on ice. Virus-bound cells were rapidly warmed to 37°C, and NH_4Cl (50 mM) was added at indicated times (up to 80 min). Cells were subsequently incubated at 37°C and harvested 7 hr after the warm shift.

Temperature Dependence

Virus binding (moi ~1) was synchronized on ice. Virus-bound cells were incubated at indicated temperatures in water bath for 1 hr, and NH_4Cl (50 mM) was then added to block any further penetration. Cells were subsequently shifted to 37°C and harvested 6 hr postwarming.

Statistical Analysis

The data are representative of at least three independent experiments, and values are given as the mean of triplicates ± standard deviation (SD).

SUPPLEMENTAL INFORMATION

Supplemental Information includes six figures, one table, three movies, Supplemental Experimental Procedures, and Supplemental References and can be found with this article at doi:10.1016/j.chom.2010.05.007.

ACKNOWLEDGMENTS

This work was supported by the Swiss National Research Foundation, an ERC advanced investigator grant, ETH Zurich, and a Marie Curie Intra European Fellowship to P.-Y.L. within the 7th European Community Framework Programme. We thank F. Rey and J. Huiskonen for critical reading of the manuscript, and L. Burleigh and A. Smith for proofreading this paper. We also thank J. Kusch from the Light Microscopy Centre (LMC) of ETH Zurich for assistance and J. Mercer for helpful discussions.

Received: December 5, 2009
Revised: March 16, 2010
Accepted: April 28, 2010
Published: June 16, 2010

REFERENCES

Brabec, M., Blaas, D., and Fuchs, R. (2006). Wortmannin delays transfer of human rhinovirus serotype 2 to late endocytic compartments. Biochem. Biophys. Res. Commun. *348*, 741–749.

Bucci, C., Thomsen, P., Nicoziani, P., McCarthy, J., and van Deurs, B. (2000). Rab7: a key to lysosome biogenesis. Mol. Biol. Cell *11*, 467–480.

Connolly-Andersen, A.M., Douagi, I., Kraus, A.A., and Mirazimi, A. (2009). Crimean Congo hemorrhagic fever virus infects human monocyte-derived dendritic cells. Virology *390*, 157–162.

Doxsey, S.J., Brodsky, F.M., Blank, G.S., and Helenius, A. (1987). Inhibition of endocytosis by anti-clathrin antibodies. Cell *50*, 453–463.

Dunn, W.A., Hubbard, A.L., and Aronson, N.N., Jr. (1980). Low temperature selectively inhibits fusion between pinocytic vesicles and lysosomes during heterophagy of 125I-asialofetuin by the perfused rat liver. J. Biol. Chem. *255*, 5971–5978.

Filone, C.M., Heise, M., Doms, R.W., and Bertolotti-Ciarlet, A. (2006). Development and characterization of a Rift Valley fever virus cell-cell fusion assay using alphavirus replicon vectors. Virology *356*, 155–164.

Garry, C.E., and Garry, R.F. (2004). Proteomics computational analyses suggest that the carboxyl terminal glycoproteins of Bunyaviruses are class II viral fusion protein (beta-penetrenes). Theor. Biol. Med. Model. *1*, 10.

Harbison, C.E., Lyi, S.M., Weichert, W.S., and Parrish, C.R. (2009). Early steps in cell infection by parvoviruses: host-specific differences in cell receptor binding but similar endosomal trafficking. J. Virol. *83*, 10504–10514.

Helenius, A., Kartenbeck, J., Simons, K., and Fries, E. (1980). On the entry of Semliki forest virus into BHK-21 cells. J. Cell Biol. *84*, 404–420.

Hirota, Y., Kuronita, T., Fujita, H., and Tanaka, Y. (2007). A role for Rab5 activity in the biogenesis of endosomal and lysosomal compartments. Biochem. Biophys. Res. Commun. *364*, 40–47.

Houle, S., and Marceau, F. (2003). Wortmannin alters the intracellular trafficking of the bradykinin B2 receptor: role of phosphoinositide 3-kinase and Rab5. Biochem. J. *375*, 151–158.

Jin, M., Park, J., Lee, S., Park, B., Shin, J., Song, K.J., Ahn, T.I., Hwang, S.Y., Ahn, B.Y., and Ahn, K. (2002). Hantaan virus enters cells by clathrin-dependent receptor-mediated endocytosis. Virology *294*, 60–69.

Johannsdottir, H.K., Mancini, R., Kartenbeck, J., Amato, L., and Helenius, A. (2009). Host cell factors and functions involved in vesicular stomatitis virus entry. J. Virol. *83*, 440–453.

Kaletsky, R.L., Simmons, G., and Bates, P. (2007). Proteolysis of the Ebola virus glycoproteins enhances virus binding and infectivity. J. Virol. *81*, 13378–13384.

Khor, R., McElroy, L.J., and Whittaker, G.R. (2003). The ubiquitin-vacuolar protein sorting system is selectively required during entry of influenza virus into host cells. Traffic *4*, 857–868.

Marsh, M., and Helenius, A. (1980). Adsorptive endocytosis of Semliki Forest virus. J. Mol. Biol. *142*, 439–454.

Martin, K., and Helenius, A. (1991). Transport of incoming influenza virus nucleocapsids into the nucleus. J. Virol. *65*, 232–244.

Mercer, J., Schelhaas, M., and Helenius, A. (2010). Virus entry by endocytosis. Annu. Rev. Biochem. Published online March 2, 2010.

Ohkuma, S., and Poole, B. (1978). Fluorescence probe measurement of the intralysosomal pH in living cells and the perturbation of pH by various agents. Proc. Natl. Acad. Sci. USA *75*, 3327–3331.

Overby, A.K., Pettersson, R.F., Grunewald, K., and Huiskonen, J.T. (2008). Insights into bunyavirus architecture from electron cryotomography of Uukuniemi virus. Proc. Natl. Acad. Sci. USA *105*, 2375–2379.

Pettersson, R., and Kaariainen, L. (1973). The ribonucleic acids of Uukuniemi virus, a noncubical tick-borne arbovirus. Virology *56*, 608–619.

Plassmeyer, M.L., Soldan, S.S., Stachelek, K.M., Roth, S.M., Martin-Garcia, J., and Gonzalez-Scarano, F. (2007). Mutagenesis of the La Crosse Virus glycoprotein supports a role for Gc (1066-1087) as the fusion peptide. Virology *358*, 273–282.

Prchla, E., Kuechler, E., Blaas, D., and Fuchs, R. (1994). Uncoating of human rhinovirus serotype 2 from late endosomes. J. Virol. *68*, 3713–3723.

Qian, M., Cai, D., Verhey, K.J., and Tsai, B. (2009). A lipid receptor sorts polyomavirus from the endolysosome to the endoplasmic reticulum to cause infection. PLoS Pathog. *5*, e1000465. 10.1371/journal.ppat.1000465.

Quirin, K., Eschli, B., Scheu, I., Poort, L., Kartenbeck, J., and Helenius, A. (2008). Lymphocytic choriomeningitis virus uses a novel endocytic pathway for infectious entry via late endosomes. Virology *378*, 21–33.

Ronka, H., Hilden, P., Von Bonsdorff, C.H., and Kuismanen, E. (1995). Homodimeric association of the spike glycoproteins G1 and G2 of Uukuniemi virus. Virology *211*, 241–250.

Rosenfeld, J.L., Moore, R.H., Zimmer, K.P., Alpizar-Foster, E., Dai, W., Zarka, M.N., and Knoll, B.J. (2001). Lysosome proteins are redistributed during expression of a GTP-hydrolysis-defective rab5a. J. Cell Sci. *114*, 4499–4508.

Sachse, M., Urbe, S., Oorschot, V., Strous, G.J., and Klumperman, J. (2002). Bilayered clathrin coats on endosomal vacuoles are involved in protein sorting toward lysosomes. Mol. Biol. Cell *13*, 1313–1328.

Santos, R.I., Rodrigues, A.H., Silva, M.L., Mortara, R.A., Rossi, M.A., Jamur, M.C., Oliver, C., and Arruda, E. (2008). Oropouche virus entry into HeLa cells involves clathrin and requires endosomal acidification. Virus Res. *138*, 139–143.

Schmaljohn, C., and Nichol, S. (2007). Bunyaviridae. In Virology, K.D. Fields, ed. (Philadelphia: Lippincott Williams & Wilkins), pp. 1741–1788.

Sieczkarski, S.B., and Whittaker, G.R. (2003). Differential requirements of Rab5 and Rab7 for endocytosis of influenza and other enveloped viruses. Traffic *4*, 333–343.

Simon, M., Johansson, C., Lundkvist, A., and Mirazimi, A. (2009a). Microtubule-dependent and microtubule-independent steps in Crimean-Congo hemorrhagic fever virus replication cycle. Virology *385*, 313–332.

Simon, M., Johansson, C., and Mirazimi, A. (2009b). Crimean-Congo hemorrhagic fever virus entry and replication is clathrin-, pH- and cholesterol-dependent. J. Gen. Virol. *90*, 210–215.

Stenmark, H., Parton, R.G., Steele-Mortimer, O., Lutcke, A., Gruenberg, J., and Zerial, M. (1994). Inhibition of rab5 GTPase activity stimulates membrane fusion in endocytosis. EMBO J. *13*, 1287–1296.

Tischler, N.D., Gonzalez, A., Perez-Acle, T., Rosemblatt, M., and Valenzuela, P.D. (2005). Hantavirus Gc glycoprotein: evidence for a class II fusion protein. J. Gen. Virol. *86*, 2937–2947.

von Bonsdorff, C.H., and Pettersson, R. (1975). Surface structure of Uukuniemi virus. J. Virol. *16*, 1296–1307.

van der Schaar, H.M., Rust, M.J., Chen, C., van der Ende-Metselaar, H., Wilschut, J., Zhuang, X., and Smit, J.M. (2008). Dissecting the cell entry pathway of dengue virus by single-particle tracking in living cells. PLoS Pathog. *4*, e1000244. 10.1371/journal.ppat.1000244.

Wessels, L., Elting, M.W., Scimeca, D., and Weninger, K. (2007). Rapid membrane fusion of individual virus particles with supported lipid bilayers. Biophys. J. *93*, 526–538.

White, J., Matlin, K., and Helenius, A. (1981). Cell fusion by Semliki Forest, influenza, and vesicular stomatitis viruses. J. Cell Biol. *89*, 674–679.

Yu, G.Y., and Lai, M.M. (2005). The ubiquitin-proteasome system facilitates the transfer of murine coronavirus from endosome to cytoplasm during virus entry. J. Virol. *79*, 644–648.

Zhang, M., Chen, L., Wang, S., and Wang, T. (2009). Rab7: roles in membrane trafficking and disease. Biosci. Rep. *29*, 193–209.